Controllable and Stable Quantized Conductance States in a Pt/HfO$_x$/ITO Memristor

Wuhong Xue, Yi Li, Gang Liu,* Zhuorui Wang, Wen Xiao, Kemin Jiang, Zhicheng Zhong, Shuang Gao,* Jun Ding, Xiangshui Miao, Xiao-Hong Xu,* and Run-Wei Li*

Quantum-level manipulation of atomic configuration offers a excellent platform for the construction of exotic nanostructures that exhibit unusual solid-state physics and electronic properties. One particular example is the memristor, in which the elaborate evolution of atomic point contact via local ionic processes and consequent stepwise device conductance quantization enable bottom-up design of in-memory computing with greatly increased data storage density and more efficient multi-value logic algorithm. In-depth understanding on the physics of atomic reconfiguration is achieved through comprehensive consideration of the thermodynamics and kinetics of nanoionics in memristors, based on which a general protocol of constructing atomic point contact structure with desired quantized conductance is established. Through energy-driven single-atom level oxygen manipulation in the reset process of a Pt/HfO$_x$/ITO structure, up to 32 consecutive quantized conductance states with an interval of half conductance quantum that can be sustained for over 7000 s and tuned 500 times are demonstrated for the first time, not only allowing the physical implementation of ternary logic-in-memory functions, but also providing a universal methodology for building next-generation quantum electronic devices.

1. Introduction

The approaching end of Moore's law and the ever-growing challenge of the von Neumann bottleneck in today's computing architectures have tremendously spurred the development of computation-in-memory paradigm with new electronic devices when handling data-intensive tasks.[1,2] One important attempt is the recently well explored memristor,[3–5] in which the nonlinear dynamics of the device allows on demand modulation of the conductance for direct logic operation while the capability of memorizing the new conductance state enables data storage at exactly the same physical location.[6,7] Eliminating the frequent data fetching and movement between the separated memory and processing units, memristors with the simplicity of a resistor structure can lead to extremely compact crossbar array for highly efficient hardware systems.[8,9] In particular, the elaborate evolution of the conductive filament via local ion motion and electrochemistry including foreign cations (such as Ag$^+$ and Cu^{2+} injected from electrochemically active metal electrodes) and native oxygen anions or vacancies (O^{2-} or V$_O$) are widely used to construct atomic point contacts (APCs) with quantized conductance features.[10–14] The stepwise development of device conductance in the unit of conductance quantum $G_0 = 2e^2/h = 77.5\ \mu S$ (where e is the elemental charge of electrons and h is the Planck's constant),[10] associated with the continuous yet precise atomic

Dr. W. Xue, Prof. G. Liu, Dr. K. Jiang, Prof. Z. Zhong, Dr. S. Gao, Prof. R.-W. Li
CAS Key Laboratory of Magnetic Materials and Devices
Zhejiang Province Key Laboratory of Magnetic Materials and Application Technology
Ningbo Institute of Materials Technology and Engineering
Chinese Academy of Sciences
Ningbo 315201, China
E-mail: gang.liu@sjtu.edu.cn; gaoshuang@nimte.ac.cn; runweili@nimte.ac.cn

Dr. W. Xue, Prof. X.-H. Xu
Key Laboratory of Magnetic Molecules and Magnetic Information
Materials of Ministry of Education
School of Chemistry and Materials Science
Shanxi Normal University
Linfen 041004, China
E-mail: xuxh@sxnu.edu.cn

Dr. Y. Li, Dr. Z. Wang, Prof. X. Miao
Wuhan National Research Center for Optoelectronics
School of Optical and Electronic Information
Huazhong University of Science and Technology
Wuhan 430074, China

Dr. W. Xiao, Prof. J. Ding
Department of Materials Science and Engineering
National University of Singapore
Singapore 119260, Singapore

**ADVANCED
SCIENCE NEWS**
www.advancedsciencenews.com

**ADVANCED
ELECTRONIC
MATERIALS**
www.advelectronicmat.de

reconfiguration of the conductive filament and one dimensional confinement of electron transport in the quantum constriction of APC,[15,16] greatly decorates the binary resistive switching feature of the device with intrinsic fault-tolerant and analog-to-digital conversion capability and directly engenders higher memory density through multibit or even decimal storage. Preceding the lithographic techniques that rely on much cruder top-down fabrication principle to make integrated circuits,[17] the broad-range tunability of device conductance may also significantly reduce the spatial-temporal complexity of in-memory computation through multi-value algorithm.

For the APCs in memristors, ions determine the physical state of the atomic configuration while electrons are responsible for conduction through discrete ballistic transport.[15,18,19] Slight rearrangement of mobile ions and coupled modification to the electronic structure can translate to significant variation in APCs' quantized conductance. Hence deep insight and precise control of the atomic configuration appear the most prominent requirements toward practical quantized conductance device applications.[20–22] Exploration of the quantized conductance of APCs in memristors can date back to 2005, when Aono and coworkers first demonstrated conductance quantization in solid electrolyte-based atomic switch devices.[8] Lot of efforts have since then been devoted to designing various material systems and devices that show quantized conductance features. For instance, both metal cations and oxygen anions are utilized to construct APCs through their migration, local rearrangement, and electrochemistry in insulating matrix of SiO_x, ZnO, ZrO_x, HfO_x, TiO_x, TaO_x, polyethylene oxide (PEO), amorphous carbon, etc.[9,12,23–26] Landau model was also adopted with the aim to establish a phenomenological relationship between the observed quantized conductance value and dimension of the APC structure.[27–29] Nevertheless, the basic understanding about the essence of local ion rearrangement and APC evolution dynamics is still inadequate, from aspects of both materials design and fundamental physics. The missing of certain quantized conductance states during continuous modulation and in statistic histogram, as well as their poor stability in terms of tuning accuracy, retention, and endurance (especially in the case of metal cation migration-based APCs), remain critical obstacles for practical application of quantum electronic devices.[30–37]

With these concerns, herein we have made in-depth understanding on the physics of atomic reconfiguration through comprehensively assessing the thermodynamics and kinetics of local ion motion and electrochemistry in memristors, based on which a general protocol of constructing atomic point contact structure with desired quantized conductance is established. By deliberately controlling the localized motion and electrochemistry of oxygen anions in the HfO_x insulator at its interface with the indium tin oxide (ITO) electrode, APCs with up to 32 consecutive integer multiples of $0.5 G_0$ states are constructed for the first time. These states can be received on-demand with excellent accuracy, as well as retained stably at room temperature for at least 7000 s and tuned precisely for over 500 steps. Electrical measurements and transmission electron microscope (TEM) observation confirm that the accurate control of quantized conductance arises from energy-driven single-atom level oxygen manipulation during stepwise reset of the Pt/HfO_x/ITO memristor and moderate evolution of the robust hafnium-based

APC. The realization of 32 robust quantized conductance states in the present memristor not only greatly increases the memory density through 5-bit storage scheme, but also allows the physical implementation of multi-value logic algorithms to further simplify the complexity of in-memory computing architectures.

2. Results and Discussion

To clarify the physics of atomic reconfiguration and its influence on the electron transport of APC structures, we first performed theoretical analyses on the integral effect of mobile ion variety, competition between atom (or atom cluster) deposition and concentration gradient-induced spontaneous atom diffusion, as well as feedback of device current on local atom rearrangement in HfO_x thin film devices. The HfO_x is chosen as the model material in this work, as its high-κ feature usually leads to promising device performance in memristors.[6,15,38] First-principles calculation indicates that active metal ions have low formation energy and migration barrier, for example, 1.02/0.72 eV for Ag^+ and 1.48/1.00 eV for Cu^{2+} in HfO_x matrix[39] (Figure S1, Supporting Information), respectively. With the low activation energies and high electric field across the device (≈MV cm^{-1}), metal ions will be injected heavily and rapidly from the electrodes into the dielectrics through hafnium vacancies, giving rise to overgrowth of the APC structure. Consequence of uncontrolled APC formation includes conductance overshoot in the current–voltage (I–V) characteristics of the devices, as well as missing of some or even all quantized conductance states during continuous modulation.[32–36] With the significant concentration gradient of foreign components established between the as-formed APC structure and the surrounding HfO_x matrix, metal atom fluctuation may also occur through thermal diffusion (e.g., via Rayleigh instability model).[29,33] Spontaneous reduction in the APC diameter with decreased surface energy and its eventual dissolution not only leads to telegraphic noise in device conductance upon competition with APC formation,[30] but also accounts for limited lifetime of the quantized conductance states.[25,36] Moreover, the increasing device current in electroforming or set process leaves a positive feedback on APC growth, contributing additionally to the formation of stronger filaments with conductance overshoot and missing of certain quantized conductance states.[23,24,36,37] Comparatively, the manipulation of oxygen anions appears more moderate, with its vacancy formation energy and migration barrier (5.96 and 2.10 eV, respectively, Figure S1, Supporting Information) much higher than that of the Ag^+ or Cu^{2+} cations. Controllable and mild reconfiguration of the APC structure via oxygen engineering can thus be made possible with more quantized conductance states and improved retention characteristics. To avoid telegraphic noise and overshoot in device conductance, as well as potential missing of quantized conductance states during continuous modulation, reset operation with negative feedback of device current on APC evolution is more desired.

Consolidating the above concerns, we designed an asymmetric Pt/HfO_x/ITO device architecture and selected reset operation mode for atomic level reconfiguration of the APC structure (**Figure 1**). The HfO_x nanofilm was fabricated on commercial ITO/glass substrate directly by radio frequency (RF) magnetron
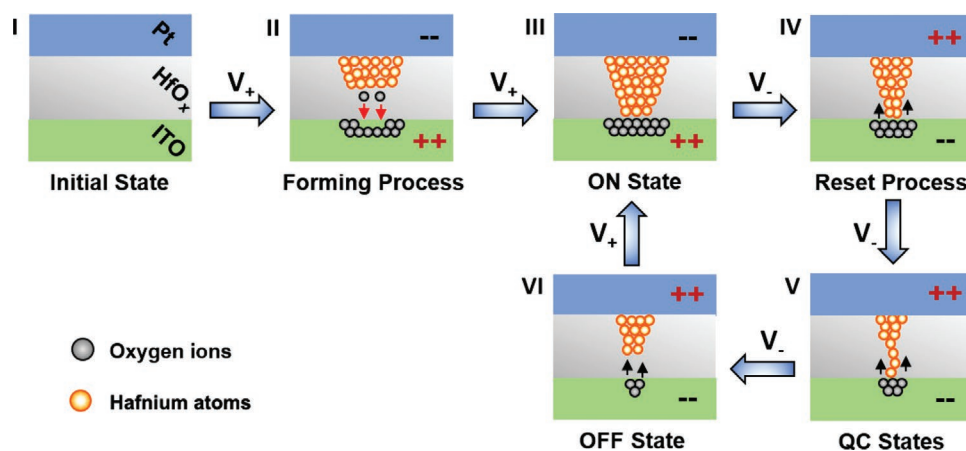
Figure 1. Schematic illustration of controlled APC evolution via oxygen ion migration in Pt/HfO$_x$/ITO asymmetric device. I) Initial state, II,III) formation of pseudo-straight conductive filament through directional oxygen cation migration in oxygen vacancy-rich region, IV,V) construction and modulation of APC in the negative-feedback reset operation, and VI) OFF state of the device.

sputtering. The as-deposited HfO$_x$ layer is monoclinic in structure, and has a thickness of ≈10 nm with root-mean-square roughness of <1 nm and O/Hf ratio of ≈2 (Figure S2, Supporting Information). The use of ITO as bottom electrode could temporarily reserve the oxygen species escaping from the switching matrix,[40–42] which assists in both forming the cone shape of the APC and maintaining the electrode complete without gas eruption (stages I–IV). Upon reversing the applied voltage polarity, oxygen anions will be injected from ITO electrode (rather than from the atmosphere) back into the HfO$_x$ matrix and recombine with the filament (stage IV). Negative feedback of the decreasing device current would limit the rate of atomic reconfiguration and thus reduce the APC size continuously. Thermally activated diffusion of oxygen anions from the surrounding oxides could also facilitate the APC shrinking, instead of making competing influence on its evolution (e.g., telegraphic noise during forming or set processes).[14] As such, accurate control of the APC size can be made possible via atom-by-atom oxygen ion manipulation, giving rise to noiseless, continuous, and stable quantized conductance phenomenon (stage V).

The APC evolution and quantized conductance feature of the Pt/HfO$_x$/ITO device was first evaluated under direct current (dc) *I–V* measurements, wherein the *I–V* curves were obtained by ramping the voltage applied to the ITO electrode and monitoring the current at a sampling rate of ≈300 counts per second. The device conductance increases slowly at the initial stage, following which multi-step transitions can be observed as the voltage exceeds 0.75 V (**Figure 2**a). Although a compliance current of 50 µA was employed to constrain the device conductance and APC dimension, back scanning of the voltage to 0 V still indicates an overgrowth of the conductive filament. Discrete quantized conductance states between G_0 and $10G_0$ are thus missing, while the device conductance progressively increases to that two orders of magnitude larger than the nominal value determined by the set voltage and compliance current.[31] Oscillation in the device conductance with an amplitude of ≈0.02G_0 occurs (Figure S3, Supporting Information), in accordance with the coexistence of electrically induced axial ion migration and thermally activated radial ion diffusion that form and break the

atomic-scale conductive channel at the boundary between the insulating and metallic states.[9,30] Such telegraphic-type fluctuations appear when the device conductance is lower than G_0, again suggesting that it is difficult in making stable APC structure via electroforming or setting the resistive switching device.

Nevertheless, complete electroforming grants the Pt/HfO$_x$/ITO device a wide switching window of ≈10^6, with the pristine OFF and ON state conductances of 3.96×10^{-10} and 6.67×10^{-4} S, respectively. Through neutralizing the strong conductive filament with oxygen anions driven by the applied electric field and concentration gradient, the wide switching window allows the reappearance of APCs during reset process (upon sweeping from 0 to −3 V, for instance) and thus a series of intermediate discrete quantized conductance states,[43] as shown in Figure 2b. To better understand such phenomenon, the tuning efficiency in APC evolution and corresponding conductance modulation were then assessed by applying successive voltage ramps with increasing maximum voltages during the reset process. The device current is found able to be continuously regulated by sweeping with a voltage ramping step of 0.01 V and deliberately tuning the sweeping stop voltage from −1.0 to −2.65 V (Figure 2c). With the device current read at a small voltage of 0.02 V after each reset operation, a clear stepwise modulation in conductance can be visualized (Figure 2d). Based on 778 reset traces and the corresponding conductance values recorded at 0.02 V from 15 devices, a cumulative histogram is statistically plotted in Figure 2e, wherein the number of quantized conductance states are counted in every 0.1G_0 step. Discrete conductance peaks, clearly concentrating at the integer multiples of 0.5G_0 in the range of 0.5G_0–16G_0, dominates the statistics and confirms the ballistic signature of charge carrier transport in a 1D constriction. In contrast to that documented in the literatures,[29,31] the probability of higher conductance values (6G_0–12G_0) only decays slightly as compared to that of lower conductance values (1G_0–4G_0), evidencing a high controllability in quantized conductance modulation. The absence of other decimal conductance between the adjacent half-integer and integer quantized conductance states also well agrees with the excellent tuning efficiency of the negative feedback reset
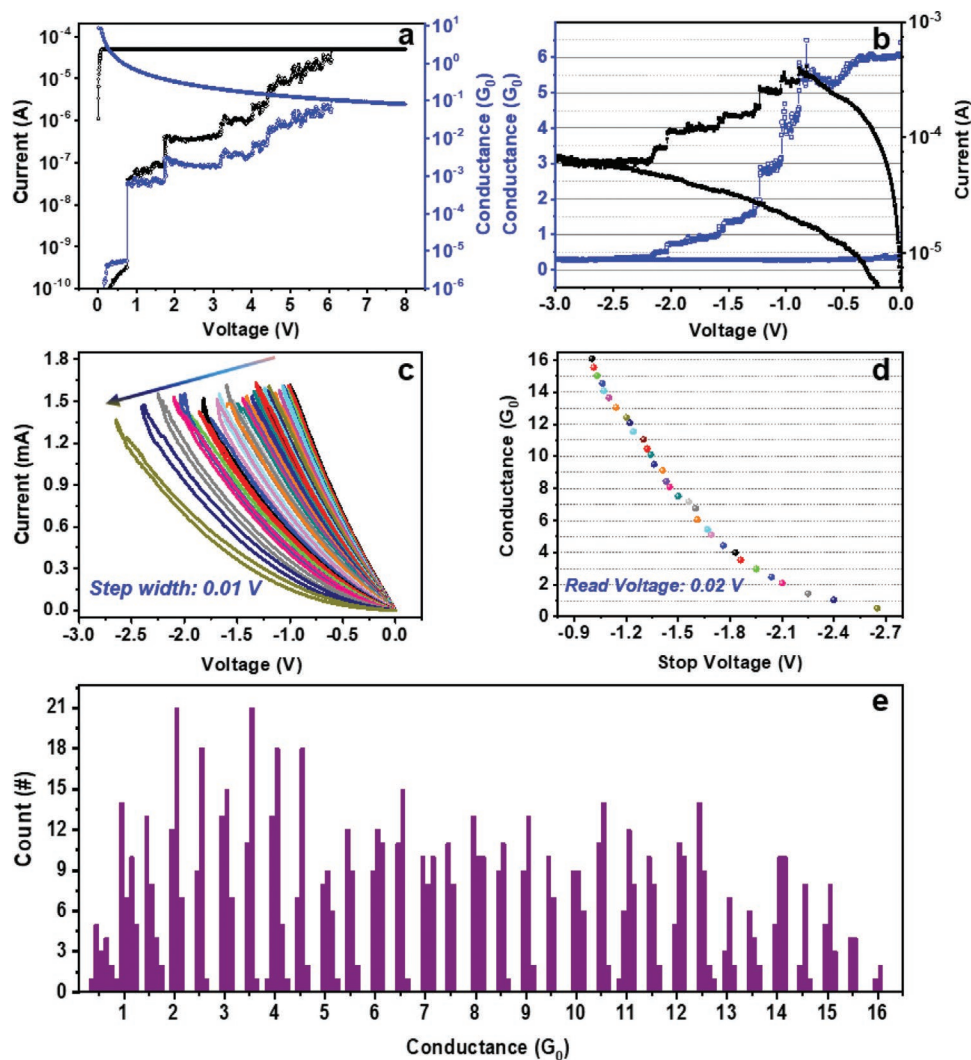
**ADVANCED
SCIENCE NEWS**
www.advancedsciencenews.com

**ADVANCED
ELECTRONIC
MATERIALS**
www.advelectronicmat.de

Figure 2. Quantized conductance feature of the Pt/HfO$_x$/ITO device. I–V characteristics during dc voltage-sweeping electroforming a) and reset b) processes. The device conductance presents oscillation in the electroforming process and a series of step changes in units of G_0 in the reset process. c) Quantized conductance modulation by dc voltage sweeping at a voltage ramping step of 0.01 V and with increasing stop voltages. d) The corresponding conductance versus stop voltage retraced from (c). e) Histogram of the device conductance retraced from 778 reset operations in 15 devices. The conductance is read at 0.02 V and quantifies into integer multiples of $0.5G_0$ from $0.5G_0$ to $16G_0$, with a total number of 32 quantized conductance states.

process on atomic reconfiguration of the APC structure. More importantly, up to 32 quantized conductance states in $0.5G_0$ unit are reported for the first time in memristors.

Notably, precise quantized conductance modulation was also demonstrated in pulse-mode reset process, wherein voltage pulses with fixed width but increasing amplitudes were used to control the atom-by-atom evolution. When the voltage pulse changes from −0.52 to −1.92 V with an increment of 0.01 V and a pulse width of 20 s, device conductance decreased stepwise from $16G_0$ to $0.5G_0$ in the unit of $0.5G_0$ (**Figure 3**a). With the full accessibility of 32 quantized conductance states during continuous operation in a single device, quantum information processing algorithm can be reliably made possible. Interestingly, quantized conductance states with higher conductance values are relatively more sensitive to the voltage stimuli, as a single pulse is capable of programming the APC to a lower state (Figure 3a). On the other hand, the voltage operating

window for conductance plateau is much wider at the lower-value quantized conductance states. That is, the regulation of APC configuration is nonlinear with regard to the applied voltages. The sensitivity of higher quantized conductance states to the applied voltage can be ascribed to the high current flowing through the APC, which accelerates the diffusion of oxygen anions from the surrounding oxides through Joule heating and facilitates the shrinking of the APC structure. Due to the same reason, the device states within the conductance range of $20G_0$–$100G_0$ can only be observed occasionally in the present study. Also, the device conductance may not be "quantized" anymore, as the charge carriers will encounter non-negligible scattering when passing through the much wider conductive filament. In other words, the charge carrier transport in these cases is no longer ballistic. With the negative feedback of device current on the atomic reconfiguration, when the APC becomes narrower and carries lower current, the rate of quantized conductance
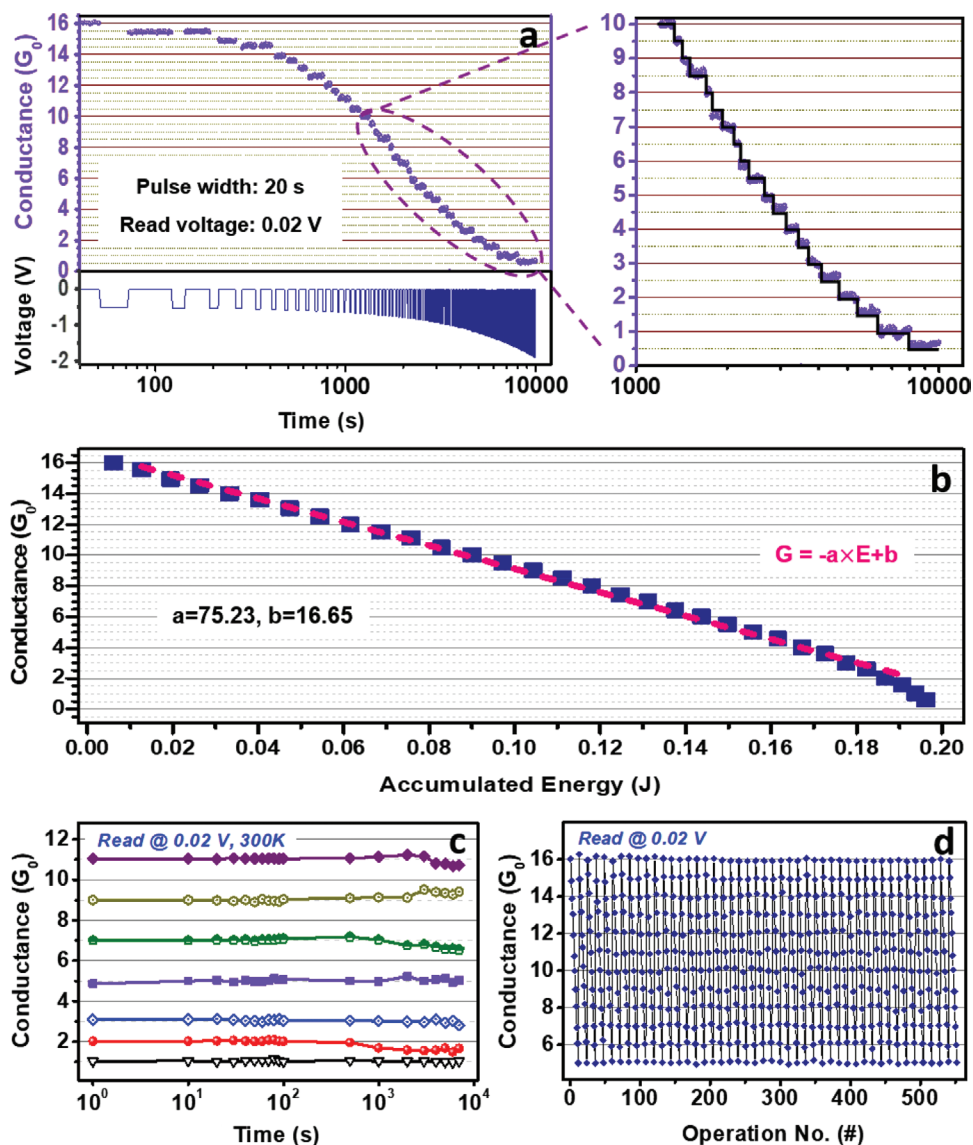
Figure 3. Precise control of quantized conductance in the Pt/HfO$_x$/ITO device. a) Quantized conductance modulation by voltage pulses with a fixed width of 20 s but increasing amplitudes. b) Conductance versus accumulated energy relationship of the device, which was calculated based on the data in (a). c) Room-temperature retention and d) endurance performance of the quantized conductance states, respectively. In all experiments, the device conductance is read at 0.02 V.

modulation slows down. Moreover, summing up the energy imposed onto the device gives a linear relationship.

$$G = -a \times E + b \qquad (1)$$

where G is the device conductance, E is the accumulated energy used to change the device conductance states, a is a constant that represents the ease of conductance modulation, and b is the device initial conductance (Figure 3b). This linear relationship clearly reveals that the on-demand controllability of the consecutive quantized conductance modulation and the elimination of conductance overshoot or missing can be ascribed to the precise energy input applied onto the device that drives the migration and electrochemistry of oxygen anions during reset process inside the HfO$_x$ insulating layer.

Further electrical measurements were performed to elucidate the dynamics of atomic reconfiguration via oxygen anion motion and electrochemistry. The same device was initially programmed to quantized conductance states with the conductance value of $\approx 8G_0$, and then stressed with various constant voltages (Figure S4a, Supporting Information). Under the stressing voltage of -0.2 V, the device conductance remains $\approx 8G_0$ with only ignorable discrepancy in the time scale of 7200 s. When the stressing voltage increases to -0.3 V, steep decreasing of the device conductance occurs at about 710 and 1120 s, respectively, suggesting that the atomic reconfiguration of APC structure is an energy-driven rather than a voltage (or electric field)-driven process. Otherwise, the resistance change would immediately occur upon the introducing of external voltage of -0.3 V that exceeds the threshold value, without the appearance of any

conductance plateau existing in the conductance–time (G–t) curve. Further increase in the stressing voltage to −0.5 V yields faster decay in device conductance. In dc sweeping mode, shortening in the voltage ramping step also modulates the device conductance more effectively.[33,42] As plotted in Figure S4b,c, Supporting Information, sweeping with smaller voltage ramping step of 0.005 V can set the device conductance to a much lower level within the same voltage operating regimes, again confirming the energy-driven nature of atomic reconfiguration. Accurately controlling the physicochemical behavior of ionic species on single-atom level not only reduces device variation for performance improvement, but also enforces the predicable creation of APC structures showing higher functional density and exotic solid-state physics and electronic phenomena. It should be noted that the appearance of quantized conductance with half-integer multiples of G_0 is not universal in all APCs and memristors. The half-integer multiples of G_0 was suggested to be caused by the chemical potential difference between the left and right carrier reservoirs or the APC configuration rearrangement.[12,29] Besides, the absence of spin degeneracy may also contribute to such phenomenon since oxygen vacancies can sometimes cause a weak magnetism.[27]

Retention and endurance characteristics are the other two critical factors in evaluating the performance of quantized conductance states. The programmed quantized conductance states ($1G_0$, $2G_0$, $3G_0$, $5G_0$, $7G_0$, $9G_0$, and $11G_0$) possess excellent retention over 7000 s at room temperature, as well as can be sustained at 125 °C for >1000 s (Figure 3c and Figure S5, Supporting Information). Since 125 °C is higher than the typical working temperature of 85 °C in modern integrated circuits, the as-received atomic point contacts in Pt/HfO$_x$/ITO memristor could satisfy the thermal stability requirement for practical device applications. Meanwhile, the quantized conductance states can be continuously and accurately modified in more than 500 operations with the conductance varying in less than $0.5G_0$ (Figure 3e), suggesting a high feasibility of controlling the APC configuration via oxygen engineering in memristors. Herein, the missing of quantized conductance states of <$5G_0$ is because the needed larger operating voltages can easily make the device broken down via the so-called negative set process, which could be avoided in future through, for example, interface engineering.[44,45]

Control experiments on devices with geometries of Ag/HfO$_x$/Pt, Cu/HfO$_x$/Pt, and Pt/HfO$_x$/Pt were conducted to corroborate the strategy of constructing APCs through oxygen ion engineering during the negative-feedback reset process of memristors. The deposition procedures of HfO$_x$ layers were identical in all these devices. Due to the much lower formation and migration energies in the HfO$_x$ matrix, severe electrode injection and fast transport of Ag$^+$ cations directly generate wide conductive filament rather than form APC structures. Sharp current jump and bistable electrical switching occurs at small voltages of about 0.1 and −0.05 V, without either the electroforming process or quantized conductance phenomenon (Figure S6a, Supporting Information). As for the case of devices with Cu top electrodes, even though quantized conductance states can be obtained in the reset process, easy re-activation of the metal ions and their massive loss from the APC lead to rapid drop in device conductance, as well as missing of certain

quantized conductance states (Figure S6b, Supporting Information). Obvious fluctuation in device conductance over $1.5G_0$ also exists during retention tests (Figure S6c, Supporting Information), which can be attributed to the structural instability of the APC arising from spontaneous diffusion of foreign metallic species into the surrounding dielectric under large concentration gradient. Nevertheless, with chemically inert Pt as both the top and bottom electrodes, the absence of oxygen reservoir function cannot provide continuous and reliable oxygen anion supply from the electrode. The APCs can only be reconfigured with oxygen ions from the surrounding oxide matrix or from the environmental atmosphere, while their back diffusion resembles telegraphic noise and missing of certain quantized conductance states in I–V characteristics (Figure S6d, Supporting Information). It is thus evident that the atomic control of oxygen species via the negative-feedback reset process in an asymmetric device offers a simple yet effective methodology for the construction of APC structures.

To better understand the controllability and stability of quantized conductance obtained in the Pt/HfO$_x$/ITO device, high-resolution TEM (HRTEM) analysis was performed to illustrate the geometry and composition of the conductive nano filaments formed in the switching matrix (**Figure 4**). Since APCs are tiny in size and cannot be easily observed in oxygen anion-dominated resistive switching devices, the Pt/HfO$_x$/ITO device was programmed to highly conductive states with potentially stronger conductive filaments for the ease of experimental observation. As shown, majority phase of the pristine HfO$_x$ thin film was identified with a monoclinic structure, showing lattice fringe of (−111) crystal planes and a d-spacing of 0.31 nm of HfO$_2$ (Figure 4a).[46] After the device was electroformed with a high compliance current of 0.01 A (Figure S7, Supporting Information), both partially and fully electroformed conductive nano filaments are observed. The partially formed nano protrusion has a sharp conical shape, as marked with the pink dotted line in Figure 4b. When fully developed, the conductive filament becomes trapezium-like (Figure 4c), with its wider and narrower diameters of about 30 and 5 nm, respectively. Zoom-in view of the lattice fringes and fast Fourier transformed images suggest that both the partially and fully developed conductive filaments consist of hexagonal hafnium showing (002) crystal plane with the d-spacing of 0.25 nm.[47] Meanwhile, temperature-independent conduction was observed in these quantized conductance states (Figure S8, Supporting Information), which not only confirms their ballistic transport nature, but also suggests that the APC merely varies in dimension while maintaining the same composition of hafnium in different quantized conductance states. The high melting point of hafnium is also responsible for the much enhanced retention of quantized conductance states in the present device.[38]

Finally, we demonstrate that the broad-range tunability of the robust quantized conductance characteristics in the present device can be utilized to physically implement multi-value logic operation with greatly reduced spatial and temporal complexity in the in-memory computing.[48] Atomic-level reconfiguration of the conductive filament and APC structure also allows ultrafast and low power operation, as documented in the literatures,[4,10,49] for very large-scale integrated circuit applications. As the simplest integral multi-value logic algorithm which is
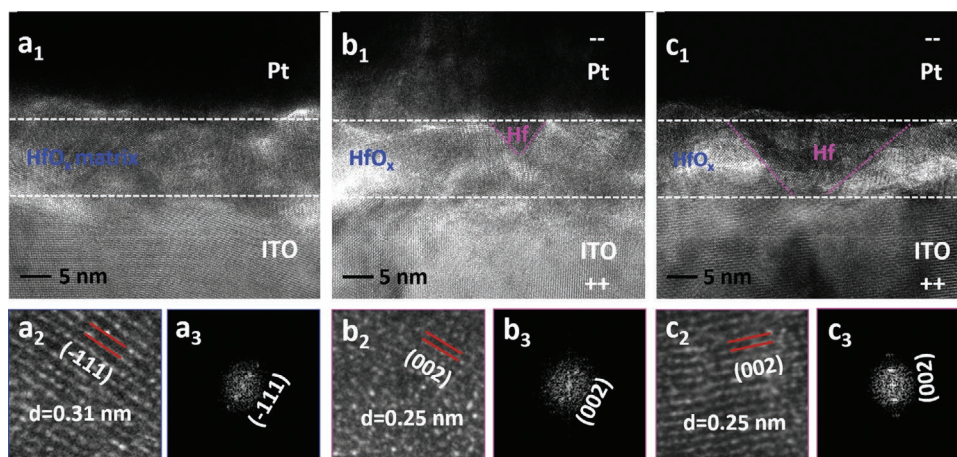
**ADVANCED
SCIENCE NEWS**
www.advancedsciencenews.com

**ADVANCED
ELECTRONIC
MATERIALS**
www.advelectronicmat.de

Figure 4. HRTEM analysis of the HfO_x switching matrix showing partially and fully developed conductive filaments. Cross-sectional HRTEM images, zoom-in view of lattice fringes, and fast Fourier transformed images of a) the pristine HfO_x thin film sandwiched between Pt and ITO electrodes, b) a partially formed conductive filament (i.e., conical nano protrusion) in the electroformed device, and c) a fully developed trapezium conductive filament in the electroformed device, respectively.

closest to the binary counterparts, ternary logic is considered promising to replace the traditional binary logic.[50] For demonstration, we designed a computationally complete ternary logic algorithm set based on the obtained quantized conductance modulation characteristics in the present $Pt/HfO_x/ITO$ device (Figure S9, Supporting Information), which includes the following functions of (2) Plus MAX, (3) Multiply MIN, and (4) Threshold Comparison.

$$f(x) = \max(a, b) \tag{2}$$

$$f(x) = \min(a, b) \tag{3}$$

$$f_k(x) = \begin{cases} 2, & x = k \\ 0, & x \neq k \end{cases} \tag{4}$$

where a and b are logic inputs and k corresponds to logic states of "0," "1," or "2." To elucidate the detail logic operation, the input logic signals "p" and "q" are defined by the terminal voltages ($V_{T2} = V_{T1} - V_T$, V_{T1}: base voltage, V_T: test voltage, V_{T2}: logic voltage), but the logic outputs are represented by the quantized conductance states of the device. Low voltage pulse (LVP: 0 V) and high quantized conductance (HQC: $11G_0$) are defined as logic "0," middle voltage pulse (MVP: 0.8 V), and middle quantized conductance (MQC: $5G_0$) are defined as logic "1" while high voltage pulse (HVP: 1.1 V) and low quantized conductance (LQC: $2G_0$) are defined as logic "2." As shown in Figure 3d and Figure S5, Supporting Information, the selected $11G_0$, $5G_0$, and $2G_0$ quantized conductance states show good retention and endurance performance for practical applications. With these definitions, both the MAX (find maximum) and MIN (find minimum) logics can be implemented within three steps of (1)) initializing the device to HQC, (2)) inputting logic signal p (V_{T2}), and (3)) inputting logic signal q (V_{T2}). For instance, when the input p and q are 00 (LVP/LVP), 01 (LVP/MVP), 02 (LVP/HVP), 10 (MVP/LVP), 11 (MVP/MVP), 12 (MVP/HVP),

20 (HVP/LVP), 21 (HVP/MVP), 22 (HVP/HVP) with V_{T1} of 0 V, the resultant QC readouts of the device are "0," "1," "2," "1," "1," "2," "2," "2," and "2," respectively, giving rise to the MAX operation according to the above function (2) (**Figure 5**a). When the input signals are 00 (LVP/LVP), 01 (LVP/MVP), 02 (LVP/HVP), 10 (MVP/LVP), 11 (MVP/MVP), 12 (MVP/HVP), 20 (HVP/LVP), 21 (HVP/MVP), 22 (HVP/HVP) with V_{T1} of 0 V for input p and 1.55 V for input q, the respective QC readouts of "0," "0," "0," "0," "1," "1," "0," "1," and "2" and above function (3) enable the MIN logic accordingly (Figure 5b).

To implement the threshold comparisons of $f_0(x)$, $f_1(x)$ and $f_2(x)$, two operations of device conductance initialization and logic signal inputting are involved. For the case of $f_0(x)$ with the base voltage of 1.2 V for V_{T2}, when the input is "0," the output logic is "2." When the inputs is either "1" or "2", the output is always "0" (Figure S10, Supporting Information). The demonstration of $f_1(x)$ involves two serially connected devices D1 and D2 that are initialized to LQC ("2"). Experimentally, when inputting the logic signal "0," "1," and "2" in the D1 and D2 with test signal $V_{TD1} = V_{T1} - V_{T2}$ (V_{T1}: base voltage of 1.1 V, V_{T2}: logic signal) and $V_{TD2} = V_{T2} - V_{T3}$ (V_{T2}: logic signal, V_{T3}: base voltage of 0.1 V), the corresponding QC readouts are "0," "2," and "0," respectively (Figure S11, Supporting Information). Finally, with the base voltage V_{T1} of 1.8 V, the input logic signals of "0," "1," and "2" give rise to the readout of "0," "0," and "2," respectively, thus matching the truth table of threshold operation $f_2(x)$ (Figure S12, Supporting Information). Theoretically, any ternary operation can be implemented by synthesizing the above computationally complete set via logic cascading, which also permits the downward compatibility with conventional binary Boolean logics.

3. Conclusion

To summarize, deep understanding on the physics of atomic reconfiguration and its influence on electron transport of the APC were obtained by comprehensively considering the integral effect of mobile ion variety, competition between atom deposition
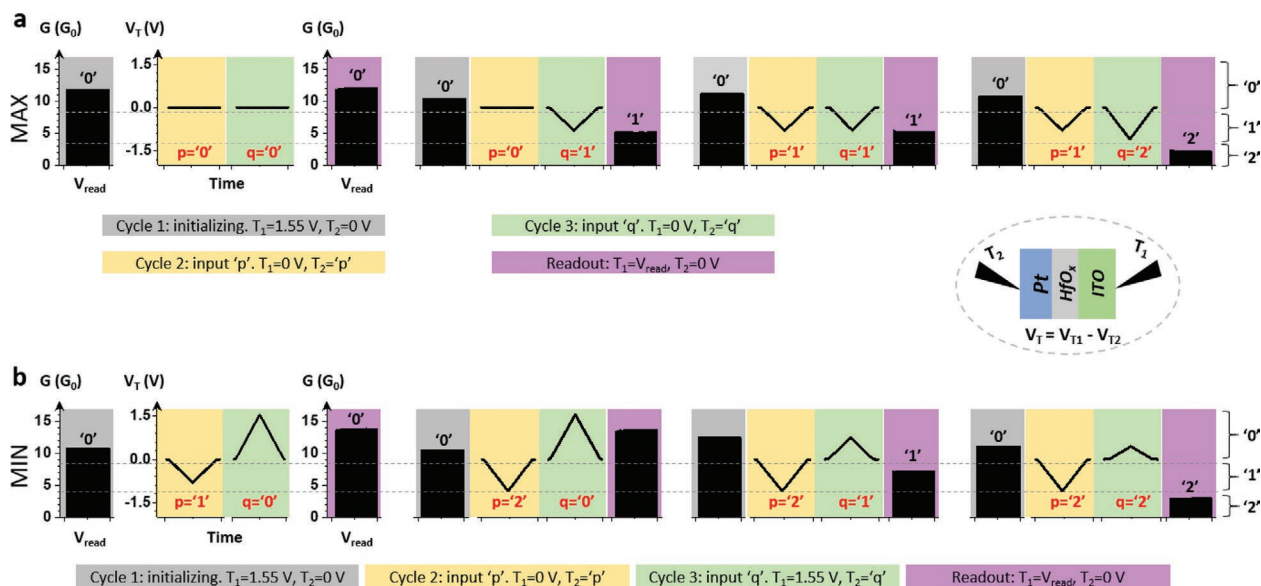
Figure 5. Proof-of-concept implementation of the MAX and MIN operations of the ternary logic algorithms based on quantized conductance characteristics of the Pt/HfO$_x$/ITO device. a) Experimentally demonstration of ternary MAX logic at four conditions ($p = q = $ '0'; $p = $ '0', $q = $ '1'; $p = q = $ '1'; $p = $ '1', $q = $ '2'). b) Experimental demonstration of ternary MIN logic at four conditions ($p = $ '1', $q = $ '0'; $p = $ '2', $q = $ '0'; $p = $ '2', $q = $ '1'; $p = q = $ '2'). Three logic cycles are required to implement these two ternary logic functions. The quantized conductance states are labeled in black histogram and the voltages applied to electrodes in each cycle are plotted in lines.

and diffusion, as well as feedback of device current on local atom rearrangement in HfO$_x$ thin film devices. Through deliberately controlling the energy-driven motion and electrochemistry of oxygen anions on single-atom level in HfO$_x$ at its interface with ITO electrode, APC showing up to 32 consecutive quantized conductance states with the interval of $0.5G_0$ is constructed via resetting the Pt/HfO$_x$/ITO memristor, which can theoretically be applied to other oxide-based memristors. Eliminating the telegraphic noises, conductance overshoot, missing, and instability issues, these 32 quantized conductance states can be received in both dc sweeping and pulse operations, as well as retained stably at room temperature for at least 7000 s and tuned precisely for over 500 steps. As such, a general protocol of constructing APC with desired quantized conductance is established, permitting multibit storage with greatly increased memory density and high performance multi-value logic-in-memory computation.

4. Experimental Section

Sample Preparation: A high-purity HfO$_2$ ceramic target (99.995%) with diameter of 2 in. and thickness of 3 mm was used for sputtering. The 10 nm HfO$_x$ film was deposited on commercial ITO/glass and Pt/Ti/SiO$_x$/Si substrates by RF magnetron sputtering technique (JGP450 system, SKY Technology CAS) at room temperature with a base pressure of lower than 1.2×10^{-4} Pa. High-purity Ar (99.999%) and O$_2$ (99.999%) with the Ar/O$_2$ ratio of 5:1 were introduced into the chamber during deposition. The RF power and working pressure were fixed at 60 W and 1 Pa during the sputtering process, respectively. The Pt top electrodes (TE), as well as the Ag and Cu TEs in the control experiments, were deposited by electron beam evaporation technique (ULVAC, MUE-ECO) at room temperature, with a diameter of 100 μm through shadow mask.

Characterization: The crystalline structure of the as-deposited HfO$_x$ films was investigated by X-ray diffraction (XRD) analysis (Bruker AXS, D8 Discover) using Cu-K$_\alpha$ radiation. Scanning probe microscopy (Veeco,

Dimension 3100 V) was employed for morphology measurements of the HfO$_x$ layer. X-ray photoelectron spectroscopic analysis (XPS, SHIMADZU, AXIS ULTRA DLD) of the HfO$_x$ layer was performed to investigate the film composition. A monochromatic Al-K$_\alpha$ X-ray source (1486.6 eV photons) was used at a constant dwell time of 100 ms. A pass energy of 80 or 40 eV was employed for the wide and core-level spectra scan, respectively. The X-ray source was run at a reduced power of 150 W (15 kV and 10 mA). The pressure in the analysis chamber was maintained at 10^{-8} Torr or lower during each measurement. The core-level signals were recorded at a photoelectron take-off angle (α, measured with respect to the sample surface) of 90°. All binding energies were referenced to the C 1s hydrocarbon peak at 284.6 eV. Surface stoichiometry was determined from XPS spectral area ratios and was reliable within ±5%. The elemental sensitivity factors were calibrated using stable binary compounds of well-established stoichiometry. Background correction and peak fit features were performed to the data using CASA XPS software. Cross-sectional HRTEM and STEM images with EDS and EELS of the samples were recorded on a FEI Titan Themis 200 transmission electron microscope by SAE Magnetics (H.K.) Ltd. Spatial resolutions of the HRTEM and STEM observations were 0.1 and 0.08 nm, respectively. The TEM specimens were prepared on a FEI Helios 450S dual beam focus ion beam (FIB) workstation with the dimension of 500 nm × 3 μm × 40 nm (height × width × thickness). Electrical characteristics of the device were recorded on a Lakeshore probe station with a Keithley 4200 semiconductor parameter analyzer. The biased voltage was applied onto the ITO bottom electrode while the Pt top electrode was grounded.

Supporting Information

Supporting Information is available from the Wiley Online Library or from the author.

Conflict of Interest

The authors declare no conflict of interest.

Keywords

[1] M. A. Zidan, J. P. Strachan, W. D. Lu, *Nat. Electron.* **2018**, *1*, 22.

[2] Z. Wang, S. Joshi, S. Savel'ev, W. Song, R. Midya, Y. Li, M. Rao, P. Yan, S. Asapu, Y. Zhuo, H. Jiang, P. Lin, C. Li, J. H. Yoon, N. K. Upadhyay, J. Zhang, M. Hu, J. P. Strachan, M. Barnell, Q. Wu, H. Wu, R. S. Williams, Q. Xia, J. J. Yang, *Nat. Electron.* **2018**, *1*, 137.

[3] R. Waser, M. Aono, *Nat. Mater.* **2007**, *6*, 833.

[4] J. J. Yang, D. B. Strukov, D. R. Stewart, *Nat. Nanotechnol.* **2013**, *8*, 13.

[5] H. S. Wong, S. Salahuddin, *Nat. Nanotechnol.* **2015**, *10*, 191.

[6] S. Kumar, J. P. Strachan, R. S. Williams, *Nature* **2017**, *548*, 318.

[7] P. Huang, J. Kang, Y. Zhao, S. Chen, R. Han, Z. Zhou, Z. Chen, W. Ma, M. Li, L. Liu, X. Liu, *Adv. Mater.* **2016**, *28*, 9758.

[8] Z. Wang, S. Joshi, S. E. Savel'ev, H. Jiang, R. Midya, P. Lin, M. Hu, N. Ge, J. P. Strachan, Z. Li, Q. Wu, M. Barnell, G.-L. Li, H. L. Xin, R. S. Williams, Q. Xia, J. J. Yang, *Nat. Mater.* **2017**, *16*, 101.

[9] J. Borghetti1, G. S. Snider, P. J. Kuekes, J. J. Yang, D. R. Stewart, R. S. Williams, *Nature* **2010**, *464*, 873.

[10] K. Terabe, T. Hasegawa, T. Nakayama, M. Aono, *Nature* **2005**, *433*, 47.

[11] W. Yi, S. E. Savel'ev, G. Medeiros-Ribeiro, F. Miao, M.-X. Zhang, J. J. Yang, A. M. Bratkovsky, R. S. Williams, *Nat. Commun.* **2016**, *7*, 11142.

[12] K. Krishnan, M. Muruganathan, T. Tsuruoka, H. Mizuta, M. Aono, *Adv. Funct. Mater.* **2017**, *27*, 1605104.

[13] S. R. Nandakumar, M. Minvielle, S. Nagar, C. Dubourdieu, B. Rajendran, *Nano Lett.* **2016**, *16*, 1602.

[14] S. U. Sharath, S. Vogel, L. Molina-Luna, E. Hildebrandt, C. Wenger, J. Kurian, M. Duerrschnabel, T. Niermann, G. Niu, P. Calka, M. Lehmann, H.-J. Kleebe, T. Schroeder, L. Alff, *Adv. Funct. Mater.* **2017**, *27*, 1700432.

[15] D. P. E. Smith, *Science* **1995**, *269*, 371.

[16] N. Agraït, *Phys. Rep.* **2003**, *377*, 81.

[17] M. M. Waldrop, *Nature* **2016**, *530*, 144.

[18] F. Q. Xie, L. Nittler, C. Obermair, T. Schimmel, *Phys. Rev. Lett.* **2004**, *93*, 128303.

[19] W. Xue, S. Gao, J. Shang, X. Yi, G. Liu, R.-W. Li, *Adv. Electron. Mater.* **2019**, *5*, 1800854.

[20] J. Lee, W. D. Lu, *Adv. Mater.* **2018**, *30*, 1702770.

[21] T. Hasegawa, K. Terabe, T. Tsuruoka, M. Aono, *Adv. Mater.* **2012**, *24*, 252.

[22] S. Long, L. Perniola, C. Cagli, J. Buckley, X. Lian, E. Miranda, F. Pan, M. Liu, J. Suñé, *Sci. Rep.* **2013**, *3*, 2929.

[23] X. Zhu, W. Su, Y. Liu, B. Hu, L. Pan, W. Lu, J. Zhang, R.-W. Li, *Adv. Mater.* **2012**, *24*, 3941.

[24] C. Hu, M. D. McDaniel, A. Posadas, A. A. Demkov, J. G. Ekerdt, E. T. Yu, *Nano Lett.* **2014**, *14*, 4360.

[25] X. Zhao, H. Xu, Z. Wang, L. Zhang, J. Ma, Y. Liu, *Carbon* **2015**, *91*, 38.

[26] G. Du, H. Li, Q. Mao, Z. Ji, *J. Phys. D: Appl. Phys.* **2016**, *49*, 445105.

[27] Y. Li, S. Long, Y. Liu, C. Hu, J. Teng, Q. Liu, H. Lv, J. Suñé, M. Liu, *Nanoscale Res. Lett.* **2015**, *10*, 420.

[28] E. Tekman, S. Ciraci, *Phys. Rev. B* **1991**, *43*, 7145.

[29] A. Mehonic, A. Vrajitoarea, S. Cueff, S. Hudziak, H. Howe, C. Labbé, R. Rizk, M. Pepper, A. J. Kenyon, *Sci. Rep.* **2013**, *3*, 2708.

[30] D. Ielmini, F. Nardi, C. Cagli, *Appl. Phys. Lett.* **2010**, *96*, 053503.

[31] C. Chen, S. Gao, F. Zeng, G. Y. Wang, S. Z. Li, C. Song, F. Pan, *Appl. Phys. Lett.* **2013**, *103*, 043510.

[32] T. Tsuruoka, T. Hasegawa, K. Terabe, M. Aono, *Nanotechnology* **2012**, *23*, 435705.

[33] S. Gao, F. Zeng, C. Chen, G. Tang, Y. Lin, Z. Zheng, C. Song, F. Pan, *Nanotechnology* **2013**, *24*, 335201.

[34] A. Mehonic, S. Cueff, M. Wojdak, S. Hudziak, C. Labbé, R. Rizk, A. J. Kenyon, *Nanotechnology* **2012**, *23*, 455201.

[35] S. Tappertzhofen, E. Linn, S. Menzel, A. J. Kenyon, R. Waser, I. Valov, *IEEE Trans. Nanotechnol.* **2015**, *14*, 505.

[36] J. J. T. Wagenaar, M. Morales-Masis, J. M. van Ruitenbeek, *J. Appl. Phys.* **2012**, *111*, 014302.

[37] F. G. Aga, J. Woo, J. Song, J. Park, S. Lim, C. Sung, H. Hwang, *Nanotechnology* **2017**, *28*, 115707.

[38] J. Shang, G. Liu, H. Yang, X. Zhu, X. Chen, H. Tan, B. Hu, L. Pan, W. Xue, R.-W. Li, *Adv. Funct. Mater.* **2014**, *24*, 2171.

[39] S. Sonde, B. Chakrabarti, Y. Liu, K. Sasikumar, J. Lin, L. Stan, R. Divan, L. E. Ocola, D. Rosenmann, P. Choudhury, K. Ni, S. K. R. S. Sankaranarayanan, S. Dattad, S. Guha, *Nanoscale* **2018**, *10*, 9441.

[40] J. Chen, K.-C. Chang, T.-C. Chang, T.-M. Tsai, C.-H. Pan, R. Zhang, J.-C. Lou, T.-J. Chu, C.-H. Wu, M.-C. Chen, Y.-C. Hung, Y.-E. Syu, J.-C. Zheng, S. M. Sze, *IEEE Electron Device Lett.* **2015**, *36*, 1138.

[41] P.-H. Chen, K.-C. Chang, T.-C. Chang, T.-M. Tsai, C.-H. Pan, T.-J. Chu, M.-C. Chen, H.-C. Huang, I. Lo, J.-C. Zheng, S. M. Sze, *IEEE Electron Device Lett.* **2016**, *37*, 280.

[42] A. Younis, D. Chu, S. Li, *J. Mater. Chem. C* **2014**, *2*, 10291.

[43] W. Banerjee, H. Hwang, *Adv. Electron. Mater.* **2019**, *5*, 1900744.

[44] S. Liu, N. Lu, X. Zhao, H. Xu, W. Banerjee, H. Lv, S. Long, Q. Li, Q. Liu, M. Liu, *Adv. Mater.* **2016**, *28*, 10623.

[45] J. Lee, C. Du, K. Sun, E. Kioupakis, W. D. Lu, *ACS Nano* **2016**, *10*, 3571.

[46] J. S. Quintero-García, B. A. Puente-Urbina, L. A. García-Cerda, O. S. Rodríguez-Fernández, E. Mendoza-Mendoza, *Mater. Lett.* **2015**, *159*, 520.

[47] S. Shinkai, H. Yanagisawa1, K. Sasaki, Y. Abe, *Jpn. J. Appl. Phys.* **1998**, *37*, 643.

[48] M. Seo, C. Hong, S.-Y. Lee, H. K. Choi, N. Kim, Y. Chung, V. Umansky, D. Mahalu, *Sci. Rep.* **2015**, *4*, 3806.

[49] G. I. Meijer, *Science* **2008**, *319*, 1625.

[50] J. Shim, S. Oh, D.-H. Kang, S.-H. Jo, M. H. Ali, W.-Y. Choi, K. Heo, J. Jeon, S. Lee, M. Kim, Y. J. Song, J.-H. Park, *Nat. Commun.* **2016**, *7*, 13413.